Influence of fretting wear on bladed disks dynamic analysis

E. Lemoine, F. Thouverez, C. Vincent, Daniel Nélias

Version of Record: https://www.sciencedirect.com/science/article/pii/S0301679X19306619
Manuscript_924d147d49864cb999e963cd92ec2b50

Influence of fretting wear on bladed disks dynamic analysis

E. Lemoine[a,b,c], D. Nélias[b], F. Thouverez[c], C. Vincent[a]

[a] *Safran Aircraft Engines, RPT René Ravaud - Réau, 77550 Moissy-Cramayel, France*
[b] *Univ Lyon, INSA-Lyon, CNRS UMR5259, LaMCoS, F-69621, France*
[c] *Ecole Centrale de Lyon, CNRS UMR5513, LTDS, F-69134 Ecully Cedex, France*

Abstract

Mastering physical phenomena taking place in aircraft engines is a key objective for manufacturers. Contact interfaces with dry friction in bladed-disks allows decreasing the dynamic response of the structure. Moreover, friction in the interfaces can induce fretting wear, decreasing even more the dynamic response. Combining harmonic balance method to study the dynamic behaviour, and a semi-analytical contact simulation method, allows to study the dynamic behaviour of the structure considering wear and dry friction in the interfaces. Furthermore, this method provides a computationally efficient tool to study the contact interfaces behaviour with accuracy and the dynamic response of the non-linear system.

Keywords: Non-linear forced response, Harmonic Balance Method, Semi-Analytical contact, Fretting, Wear

1. Introduction

Precise prediction of vibration levels is a key objective in order to reach noise and pollution reduction goals for aircraft engines. Mastering this topic requires to have a better understanding and control on physical phenomena taking place in the engines. Dry friction in bladed-disks contact interfaces allows decreasing the dynamic response by dissipating energy. Thanks to numerical [1, 2, 3] and experimental [4, 5, 6] studies this non linear phenomenon is now better understood. Moreover, a worn geometry induces a lower vibration level [7]. Simulation of bladed disks dynamic response considering fretting wear can then have a meaningful impact on the engine design.

This work aims at simulating the non-linear forced response of an academic bladed disk model made of two different materials, to determine the wear it induces. The non-linear forced response of the worn geometry is then re-computed to evaluate the impact of fretting wear on the vibration amplitudes and on the stresses over the interface. In order to understand accurately the phenomena taking place in the model, a detailed study of the contact behaviour is conducted at resonance. This allows studying the contact forces distribution, the stick-slip behaviour and the sliding displacements, to compute wear depth on contact interfaces.

The structure is represented by its structural matrices extracted from a commercial finite element solver, considering a fixed centrifugal preloading [8] and cyclic symmetry properties [9]. Structural matrices are then reduced using Craig-Bampton fixed-interface component mode synthesis [10], where only contact and excitation degrees of freedom (DOFs) are kept, along with the first eigenmodes of the structure. The non-linear forced response is evaluated using Harmonic Balance Method (HBM), consisting on a Galerkin procedure to express the equation of motion as an algebraic system in the frequency domain. Since contact forces have no expression in the frequency domain, an alternating frequency-time procedure [11] is used to express contact forces in the time domain. Different methods to estimate the contact forces have been studied, like penality contact elements [12]. For this study, the Dynamic Lagrangian Frequency-Time scheme (DLFT) developed by Nacivet [1] was used. This method takes Coulomb's friction law and non-interpenetration condition into account to determine contact forces in time domain. Moreover, it has already proved its validity for bladed disks dynamic analysis considering dry friction [4].

Despite its accuracy to predict the dynamic behaviour, the HBM does not allow using a fine mesh at the contact interfaces, since computation time would become prohibitive. To be able to study in detail the contact interfaces behaviour, the HBM was coupled with a semi-analytical contact solver [13, 14, 15].

The non-linear resonance state is then considered to study the interfaces. Gallego [16] proposed a semi-analytical contact simulation method to study the Low Cycle Fatigue (LCF) of the system. By coupling this method with the HBM, it is then possible to study the High Cycle Fatigue (HCF) of the system, with a vibration dynamic loading. Contact forces and moments are then extracted from the HBM solver and used as an input for the semi-analytical contact analysis. The interest of the semi-analytical contact solver is to discretise finely the interfaces and have fast computations. Moreover, by considering the coupling between the normal and tangential contact problems, two different materials in contact can be taken into account. The wear depth is then computed using a local energy based formulation [17]. Finally, the finite element geometry is updated and the whole process is re-evaluated to determine the forced response of the worn geometry. This loop is done several times to determine the global wear behaviour of the system. Since wear have a negligible impact on the structural behaviour after one dynamic cycle, the structure is updated after an important

number of cycles. The impact of wear on the stresses over the interface is then studied.

2. Studied model

2.1. Finite element model

Since the final application of this work is aircraft engines bladed-disks, this study was conducted on a simplified bladed disk model, allowing to represent the mechanical properties of an industrial bladed disk. The model is composed of 24 blades connected to the disk with dovetails contacts. The materials constituting the disk and the blades are respectively structural steel and titanium alloy. Since the 24 sectors of the disk are considered identical, cyclic symmetry properties can be applied, allowing to compute only 1 sector of the model instead of 24 [9]. Figure 1 shows the full bladed disk model and Figure 2 shows one sector with its boundary conditions.

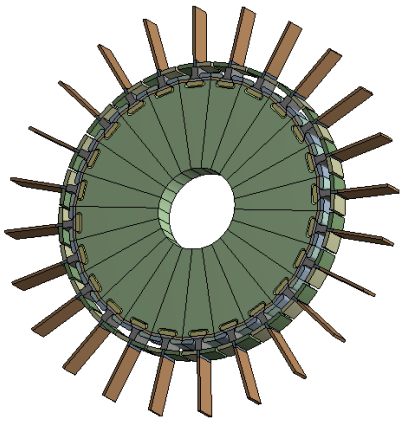

Figure 1: Full studied model

The disk bore is considered fixed. A centrifugal loading is applied on the structure by the mean of a rotation speed ω_z, leading to a centrifugal preload. The contact due to the preload is computed using Lagrange method with an explicit scheme. This centrifugal preload adds two terms to the full structural stiffness matrix $\mathbf{K}_f$: $\mathbf{K}_\omega$ and $\mathbf{K}_g$ which correspond respectively to the centrifugal softening and the geometric stiffening [18]. Those effects, as well as all the structural matrices of the system are computed using a commercial finite element (FE) solver. Two equations of motion are then constructed, one for each solid $l = 1, 2$ i.e. the disk and the blade:

$$\mathbf{M}_f^l \ddot{\boldsymbol{X}}_f^l + \mathbf{C}_f^l \dot{\boldsymbol{X}}_f^l + \mathbf{K}_f^l \boldsymbol{X}_f^l + \boldsymbol{F}_{c_f}^l = \boldsymbol{F}_{ex_f}^l , \quad l = 1, 2 . \tag{1}$$

with

$$\mathbf{K}_f^l = \mathbf{K}_{struct}^l - \mathbf{K}_\omega^l + \mathbf{K}_g^l , \quad l = 1, 2 . \tag{2}$$

The subscript $\bullet_f$ in the notations stands for "full model". $\mathbf{M}_f$ is the mass matrix, $\mathbf{C}_f$ is the damping matrix and $\mathbf{K}_f$ is the stiffness matrix made of the structural stiffness matrix $\mathbf{K}_{struct}$, the centrifugal softening matrix $\mathbf{K}_\omega$ and the geometric stiffening matrix $\mathbf{K}_g$. The vectors $\boldsymbol{X}_f$, $\boldsymbol{F}_{c_f}$ and $\boldsymbol{F}_{ex_f}$ correspond respectively to the displacements, the contact forces in the dovetail and the excitation forces used for the following dynamic study. The damping matrix $\mathbf{C}_f$ is built using a structural modal damping. Gyroscopic effects are considered negligible and hence not taken into account for this study.

Figure 2: Sector of the studied model with boundary conditions.

2.2. Craig-Bampton reduction

To reduce the size of the matrices, several reduced order modelling techniques can be used, such as component mode synthesis [10, 19, 20, 21], standard mode superposition or proper orthogonal decomposition [22]. For this study, the Craig-Bampton fixed-interface component mode synthesis [10] was performed, since it has shown its efficiency and it is widely used for non-linear dynamics problems. This method consists on reorganising the matrices in two parts: boundary DOFs (index b) and internal DOFs (index i). For this study, the boundary DOFs are the contact DOFs, one excitation node (EXC on Figure 2) and one observation node (OBS on Figure 2), both at the blade's tip. These excitation and observation nodes are kept for convenience to simplify the use of this test case even though they are not strictly required for the simulation They correspond to the degrees of freedom that are kept physical after the reduction. All the other DOFs are considered as internal DOFs. The system is then reorganised as follows:

$$\mathbf{K}_f = \begin{pmatrix} \mathbf{K}_{ii} & \mathbf{K}_{ib} \\ \mathbf{K}_{bi} & \mathbf{K}_{bb} \end{pmatrix} , \quad \mathbf{M}_f = \begin{pmatrix} \mathbf{M}_{ii} & \mathbf{M}_{ib} \\ \mathbf{M}_{bi} & \mathbf{M}_{bb} \end{pmatrix} , \quad \boldsymbol{X}_f = \begin{pmatrix} \boldsymbol{X}_i \\ \boldsymbol{X}_b \end{pmatrix} \tag{3}$$

The idea of the Craig-Bampton reduction is to approximate the solution by expanding it on the eigenmodes basis of several substructures. The Craig-Bampton transformation matrix can then be expressed as:

$$\mathbf{T} = \begin{pmatrix} \boldsymbol{\Phi} & \boldsymbol{\Psi} \\ \mathbf{0} & \mathbf{I} \end{pmatrix} \tag{4}$$

where $\mathbf{\Phi}$ is the fixed-interface modes matrix and $\mathbf{\Psi}$ the static modes matrix. The reduction of the system is made by considering only the N_m first eigenmodes in the fixed-interface modes matrix $\mathbf{\Phi}$. The system is then reduced by means of the T matrix which leads to the following reduced matrices, where index $\bullet_{CB}$ stands for Craig-Bampton reduced matrices:

$$\mathbf{K}_{CB} = \mathbf{T}^T \mathbf{K}_f \mathbf{T}\,, \quad \mathbf{M}_{CB} = \mathbf{T}^T \mathbf{M}_f \mathbf{T}\,, \quad \mathbf{F}_{ex,CB} = \mathbf{T}^T \boldsymbol{F}_{ex_f} \tag{5}$$

For this study, 15 eigenmodes were kept for the disk and 20 for the blade. The FE model was then reduced from 116250 DOFs for the full model to 629 DOFs for the reduced one. The error on the frequency of the first flexural mode of the bladed disk (studied thereafter) with bonded interface is less than 0.3% in comparison with the full finite element model.

In a matter of notation simplification, the subscript $\bullet_{CB}$ indicating the reduced Craig-Bampton model will not be mentioned thereafter, since all the computations are made on the reduced model.

3. Non-linear forced response

The dynamic study presented here was conducted on the first flexural mode of the bladed disk with a 0-diameter excitation, meaning that the excitation is the same for all blades simultaneously. The deformed shape of the mode is given in Figure 3. The methodology presented here can also be applied to the other eigenmodes of the structure

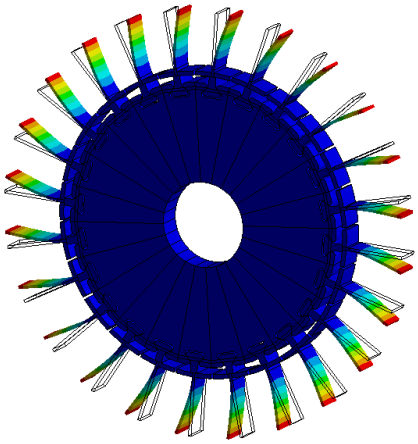

Figure 3: First flexural mode of the bladed disk

3.1. Harmonic Balance Method

To compute the non-linear forced response of a structure, an excitation is applied at the blade's tip, at the excitation node (EXC on Figure 2). By applying a periodic excitation on the system it is possible to look for a periodic solution to study the steady-state response. Therefore, the Harmonic Balance Method (HBM) can be used to solve this problem [23]. The HBM consists in using a Galerkin procedure by expanding the equations of motion in the trigonometric functions basis, truncated at the harmonic N_h. This projection leads to an algebraic expression of the equation of motion in the frequency domain:

$$\mathbf{Z}^l \tilde{\boldsymbol{X}}^l + \tilde{\boldsymbol{F}}_c^l = \tilde{\boldsymbol{F}}_{ex}^l\,, \quad l = 1, 2\,. \tag{6}$$

where $\tilde{\boldsymbol{X}}^l$, $\tilde{\boldsymbol{F}}_{\boldsymbol{c}}^{\ l}$ and $\tilde{\boldsymbol{F}}_{ex}^l$ represent respectively the multi-harmonic vectors of displacements, contact forces in the dovetail and excitation forces. $\mathbf{Z}^l$ is the dynamic stiffness matrix, which is block-diagonal and defined as:

$$\mathbf{Z}^l = \begin{bmatrix} \mathbf{K}^l & 0 & \cdots & 0 \\ 0 & \mathbf{Z}_1^l & & \vdots \\ \vdots & & \ddots & 0 \\ 0 & \cdots & 0 & \mathbf{Z}_{N_h}^l \end{bmatrix}, \tag{7}$$

$$\mathbf{Z}_k^l = \begin{bmatrix} \mathbf{K}^l - (k\omega)^2 \mathbf{M}^l & k\omega \mathbf{C}^l \\ -k\omega \mathbf{C}^l & \mathbf{K}^l - (k\omega)^2 \mathbf{M}^l \end{bmatrix}, \quad k = 1..N_h\,. \tag{8}$$

This transformation changes the unknowns of the system, which are no longer the physical displacements, but the Fourier coefficients of the displacements $\tilde{\boldsymbol{X}}^l = \left[\boldsymbol{a_0}\left(\boldsymbol{X}^l\right), \boldsymbol{a_1}\left(\boldsymbol{X}^l\right), \boldsymbol{b_1}\left(\boldsymbol{X}^l\right), ..., \boldsymbol{a}_{\boldsymbol{N_h}}\left(\boldsymbol{X}^l\right), \boldsymbol{b}_{\boldsymbol{N_h}}\left(\boldsymbol{X}^l\right)\right]^T$, with N_h the number of harmonics considered in the Fourier series.

Two additional reductions are then made on the system [1]. The first reduction consists on reorganising the matrices to keep only the non-linear DOFs, which are the contact DOFs. A second reduction is conducted to express the system in relative displacements since a contact problem is studied; leading to the following equation:

$$\mathbf{Z_r} \tilde{\boldsymbol{X}}_{\boldsymbol{r}} + \tilde{\boldsymbol{\lambda}} = \tilde{\boldsymbol{F}}_{\boldsymbol{r}} \tag{9}$$

where $\mathbf{Z_r}$ is the reduced relative stiffness matrix, $\tilde{\boldsymbol{X}}_{\boldsymbol{r}}$ is the multi-harmonic relative displacements vector, $\tilde{\boldsymbol{\lambda}}$ is the contact forces vector and $\tilde{\boldsymbol{F}}_{\boldsymbol{r}}$ is the reduced excitation force vector.

3.2. Contact forces evaluation

Solving the previous algebraic system (Equation 9) means being able to compute the contact forces $\tilde{\boldsymbol{\lambda}}$. However, there is no existing expression of the contact forces in the frequency domain. The alternating frequency-time procedure [11] is then used, consisting in using a discrete Fourier transform to estimate the contact forces in the time domain with the expression of the relative displacements, before going back to the frequency domain to evaluate equation 9. The iterative non-linear solving algorithm iterates over the relative displacement until it reaches convergence. The alternating frequency time procedure used for this study is the so called Dynamic Lagrangian Frequency Time (DLFT) procedure developed by Nacivet [1]. This contact method was developed on a node-to-node contact. The contact interfaces in this model are built with linear shape functions. It consists of adding an unknown vector $\tilde{\boldsymbol{Y}}_{\boldsymbol{r}}$ satisfying the contact laws such as $\tilde{\boldsymbol{Y}}_{\boldsymbol{r}} = \tilde{\boldsymbol{X}}_{\boldsymbol{r}}$ when the convergence is reached. Nacivet proposed to define the contact forces $\tilde{\boldsymbol{\lambda}}$ as dynamic Lagrangians, using a penalty term ϵ in the equation of motion in the frequency domain:

$$\tilde{\boldsymbol{\lambda}} = \tilde{\boldsymbol{F}}_{\boldsymbol{r}} - \mathbf{Z_r} \tilde{\boldsymbol{X}}_{\boldsymbol{r}} + \epsilon\left(\tilde{\boldsymbol{X}}_{\boldsymbol{r}} - \tilde{\boldsymbol{Y}}_{\boldsymbol{r}}\right) \tag{10}$$

The contact force $\tilde{\boldsymbol{\lambda}}$ is then computed in the time domain after splitting the equation in two parts:

$$\begin{aligned}\tilde{\boldsymbol{\lambda}} &= \tilde{\boldsymbol{F}}_r - \mathbf{Z}_\mathbf{r}\tilde{\boldsymbol{X}}_r + \epsilon\left(\tilde{\boldsymbol{X}}_r - \tilde{\boldsymbol{Y}}_r\right) \\ &= \underbrace{\tilde{\boldsymbol{F}}_r - \mathbf{Z}_\mathbf{r}\tilde{\boldsymbol{X}}_r + \epsilon\tilde{\boldsymbol{X}}_r}_{\tilde{\boldsymbol{\lambda}}_x} - \underbrace{\epsilon\tilde{\boldsymbol{Y}}_r}_{\tilde{\boldsymbol{\lambda}}_y}\end{aligned} \tag{11}$$

where $\tilde{\boldsymbol{\lambda}}_x$ is used as a prediction to determine the stick-slip behaviour of the system since every terms are known and $\tilde{\boldsymbol{\lambda}}_y$ is used as a correction term. The correction is applied by imposing its value to enforce the validation of the contact laws: unilateral contact, separation and Coulomb's friction law. More details on this method are given in [1, 4].

3.3. Dynamic response

Using HBM coupled with the DLFT procedure on the academic bladed disk model allows to obtain the non-linear dynamic response, considering dry friction in the dovetail contact. Figure 4a represents the forced response of the system for several friction coefficients μ. The discontinuous blue curve represents the linear response which is the bonded interfaces response, whereas the continuous curves represent the different non-linear (considering friction) responses. The non linear forced responses are lowered compared to the linear one, since friction in the contact interfaces dissipates energy, hence lowers the dynamic response. Moreover, the smaller the coefficient of friction μ is, the more the forced response decreases. This behaviour can be explained since a lower coefficient of friction fosters sliding in the interfaces, then more energy is dissipated, which in fine decreases the dynamic response. Plots in Figure 4 were made using an excitation amplitude $F_e = 0.2$.

In addition, by fixing the friction coefficient $\mu = 0.3$, it is possible to modify the excitation amplitude to study its influence on the damping induced by the non-linearity. Figure 4b represents the influence of the excitation amplitude on the damping. The blue curve represents the linear forced response and the other curves are the forced responses for different excitation amplitudes all normalised by their linear maximum. It can be observed that a very small amplitude leads to have the same response as the linear since the displacements are too small to induce sliding. Increasing the excitation amplitude will then encourage sliding and energy dissipation, increasing the difference between the linear and non-linear curves, which corresponds to the damping induced by the friction dissipated energy.

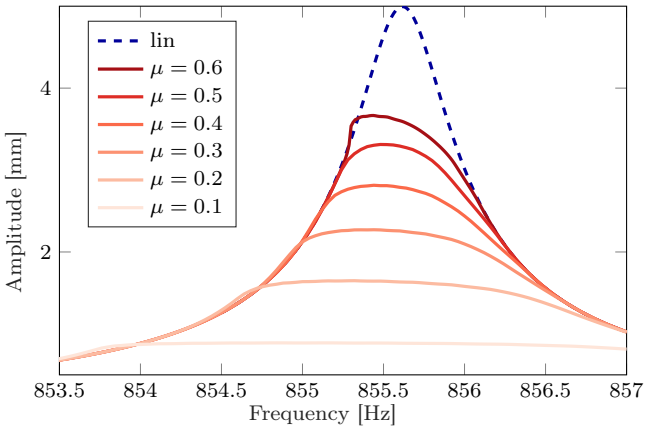

(a) Influence of the friction coefficient μ for a fixed excitation amplitude $F_e = 0.2$

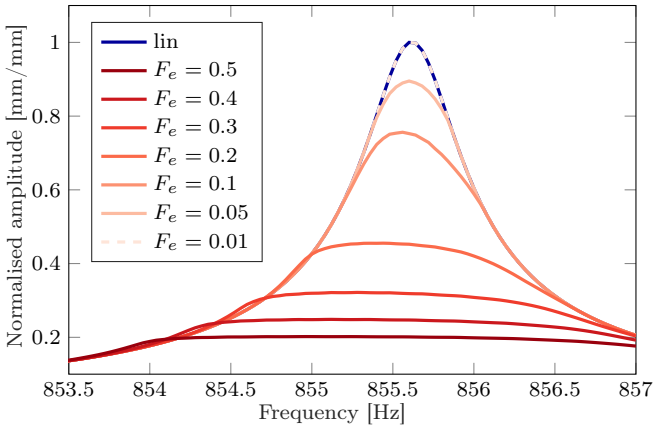

(b) Influence of the excitation amplitude on the normalised forced response for a fixed friction coefficient $\mu = 0.3$

Figure 4: Influence studies on the dynamic force response

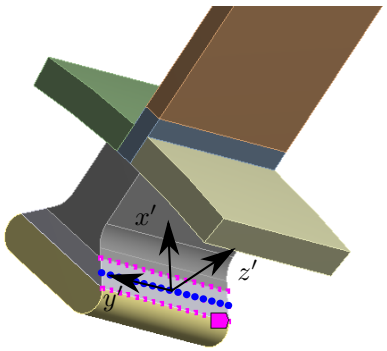

Figure 5: Nodes studied on the blade in blue and local framework (x', y', z') normal to the interface

3.4. Contact behaviour

The two previous influence studies validate the expected behaviour of the structure. Moreover, checking the contact forces and sliding computed with the DLFT allows to verify the physical consistency in the contact interfaces. Figure 6a represents the tangential load T and the normal load multiplied by the friction coefficient μN whereas Figure 6b shows the slip associated to the same nodes. Both Figures 6 correspond to the contact nodes in the middle of the interface, represented in blue in Figure 5, at one time step of the vibration period at resonance, where the loads are maximum. The coordinates are expressed in the local framework (x', y', z') normal to the interface.

Figure 6a shows that the tangential load is equal to the normal load times the friction coefficient $T = \mu N$, which validates Coulomb's friction law in the middle of the interface. Therefore, the corresponding nodes should be sliding, which is confirmed by the slip observed in the middle of the interface on

Figure 6b. Hence, the contact behaviour is validated since the efforts validate Coulomb's friction law in a zone where sliding is observed. Moreover, Figure 6a shows small side effects on the load, meaning the load increases near the side of the contact, due to the pin-plane like contact between the blade and the disk. This behaviour is characteristic of this kind of contact. However, this effect is quite small since a really gross mesh was used in this model, to keep fast dynamic computations.

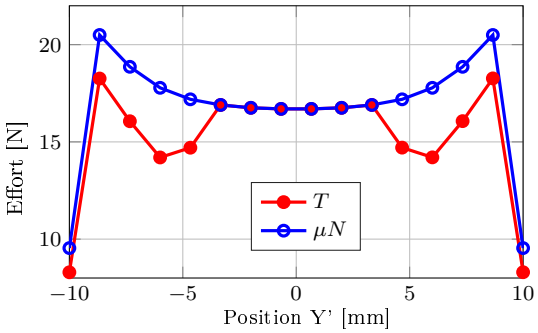

(a) Contact loads

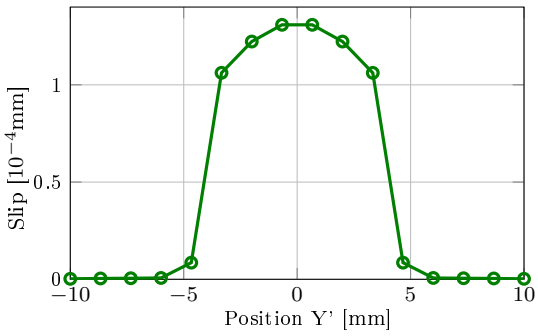

(b) Slip

Figure 6: Contact behaviour of the middle nodes of the interface at one time step of the dynamic period, computed with the DLFT.

A convergence study on the mesh validates that this mesh is sufficient to obtain the forced response of the system at blade's tip. Nevertheless, previous results show that the mesh is not sufficient to study the interfaces' behaviour accurately, mostly for the repartition of the effort and slip. Therefore, the interfaces need to be refined much more to be able to study the interfaces behaviour and compute wear. The previous dynamic study is then coupled with a semi-analytical contact solver to be able to discretise the contact interfaces.

4. Refined contact analysis

To avoid using a refined mesh in the dynamic analysis, which would increase the computation time and complexity, a semi-analytical contact resolution method [16] is used at the resonance frequency, where the load is the highest. This method allows to use a really small mesh while keeping fast computations.

4.1. Semi-analytical contact solver

The semi-analytical contact simulation method consists in determining stresses and displacements on the contact zone, by using known analytical solutions to solve a Boundary Element Method (BEM) problem [24, 25]. These solutions are built from the Green coefficients, giving the contribution of the pressure p, applied on a rectangular surface, on the elastic displacements $\bar{u}_J^p$ at the surface of a semi-infinite elastic space in the direction J such as:

$$\frac{\bar{u}_J^p}{p} = K_J^p(x, y) \tag{12}$$

Both solids are discretised and the contact behaviour is considered as having no influence on the structural response far from the contact, which means it can be considered as a semi-infinite half-space. Therefore, the Green coefficients can be used to determine the contact behaviour between the blade and the disk. Linear elasticity theory allows to superimpose the solutions for each discretised element [16]. After discretising the interfaces, the displacements of the point with (i, j) coordinates due to a loading on the surface can then be determined by adding all the contributions in both directions:

$$\bar{u}_z^p(i, j) = \sum_{l=1}^{N_x} \sum_{m=1}^{N_y} p(l) \underline{K}_z^p(l - i, m - j) \tag{13}$$

Similar equations can be expressed in all directions J for the displacements $\bar{u}_J^p$ and the stresses σ_{IJ}^p, for the pressure p and the shear forces q_x and q_y [25]. These double sums (Eq.13) are convolution products. It can then be transformed in a classical product by expressing it like wave components in space, using 2D space Fourier transform [26]. This method is detailed by Gallego [16]. Using fast Fourier transform to re-express the convolution product in a classical product in the frequency domain allows keeping fast computations even if a very fine mesh is used for the contact interfaces. Taking two different materials in contact into account implies considering the contributions of the tangential loads on the normal displacement as shown in [16]. Therefore, the full normal displacement at position (i, j) can be written as:

$$\begin{aligned} \bar{u}_z(i, j) = & \sum_{l=1}^{N_x} \sum_{m=1}^{N_y} p(l) \underline{K}_z^p(l - i, m - j) \\ & + \sum_{l=1}^{N_x} \sum_{m=1}^{N_y} q_x(l) \underline{K}_z^{q_x}(l - i, m - j) \\ & + \sum_{l=1}^{N_x} \sum_{m=1}^{N_y} q_y(l) \underline{K}_z^{q_y}(l - i, m - j) \end{aligned} \tag{14}$$

Where q_x and q_y are the tangential shear forces in the x and y directions respectively, and $\underline{K}_z^{q_x}$ and $\underline{K}_z^{q_y}$ are the Green coefficients corresponding to the contribution of the tangential shear forces in x and y directions.

By expressing the contact problem resolution as the minimisation of the complementary energy [27], the problem can be solved with a conjugate gradient algorithm [28], validating contact

laws such as Coulomb's friction law. The coupling between normal and tangential loads is then taken into account by alternating the resolution of normal and tangential problem until convergence.

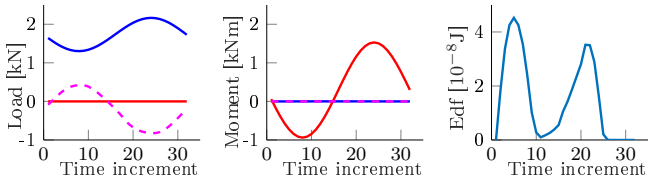

(a) Sum of loads (b) Sum of moments (c) Dissipated energy

Figure 7: Input data for the semi-analytical contact solver, extracted from the dynamic analysis in all directions: Z(——), Y(——), X(– –)

Input data for the semi-analytical contact solver is the dynamic structural behaviour extracted from the HBM computation made section 3. The input data is then the sum of the contact loads and moments in the three directions at every time-step $n = 1...Nt$ of the vibration period:

$$P^n = \sum_{N_{DOFs}} P_i^n \,, \quad Q_x^n = \sum_{N_{DOFs}} Q_{x_i}^n \,, \quad Q_y^n = \sum_{N_{DOFs}} Q_{y_i}^n \tag{15}$$

$$M_z^n = \sum_{N_{DOFs}} \left(x_i Q_{y_i} - y_i Q_{x_i} \right) \,, \quad M_x^n = \sum_{N_{DOFs}} x_i P_i^n \,, \quad M_y^n = \sum_{N_{DOFs}} y_i P_i^n \tag{16}$$

where P^n, Q_x^n and Q_y^n are respectively the total normal and tangential loads in directions x and y at time-step n. P_i^n, $Q_{x_i}^n$ and $Q_{y_i}^n$ are the local loads at node i of the contact interface in the dynamic computation. M_z^n, M_x^n and M_y^n are the total moments on the interface and x_i and y_i are the coordinates of node i. All these computations are made in the local frame normal to the interface (cf Figure 5). Finally, the friction dissipated energy E_{df}^n in the interface is added as the last input data:

$$E_{df}^n = \sum_{N_{DoFs}} \sqrt{{Q_{x_i}^n}^2 + {Q_{y_i}^n}^2}\, s_i^n \tag{17}$$

where s_i^n is the relative displacement between the blade and the disk at time-step n for the node i, which corresponds to sliding. Figure 7 represents all these input data. A convergence study was achieved over these input data showing that they were all converged with respect to the mesh from the dynamic analysis since there are integral quantities over the interface.

4.2. Detailed contact behaviour study

Using the semi-analytical contact solver with the global input data from the dynamic analysis, the load distribution over the interface can be obtained. Figure 8a represents the normal load distribution at one time-step of the vibration period. It shows that the mesh used for this calculation is much finer than the mesh used previously in the dynamic analysis. Moreover, Figure 8b represents the tangential force T and the normal force times the friction coefficient μN on the middle nodes of the interface (cf. Figure 5) and Figure 8c represents the sliding on

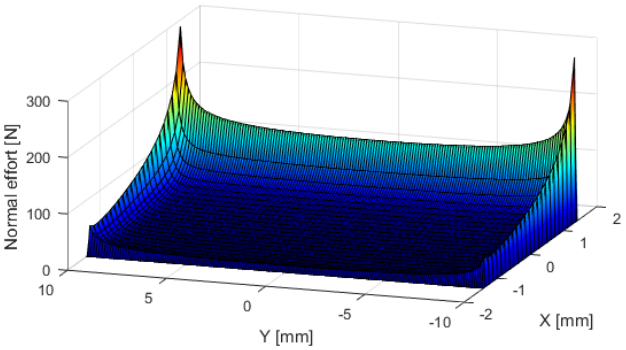

(a) Normal load repartition over the interface

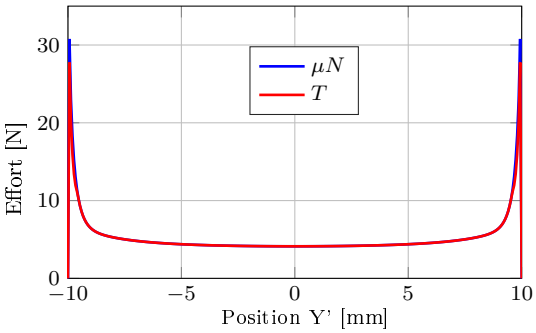

(b) Contact loads

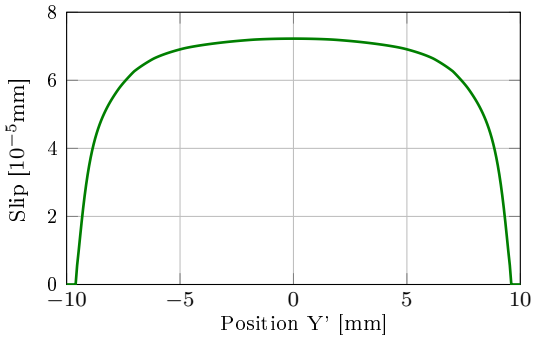

(c) Slip

Figure 8: Contact behaviour of the full surface (a) and of the middle nodes of the interface (b) and (c), at one time-step of the dynamic period, computed with the semi-analytical method.

the same nodes at the same time-step. By comparing Figures 8 with Figures 6 we can observe the same behaviour, which is stick-slip over the interface, with slip in the middle of the interface and stick in the border, where $T \neq \mu N$. Nevertheless, the edge effects are much higher with the refined mesh and the loads and slip are spread over the interface. This can be explained since the refined mesh distributes more accurately the loads: decreases the loads in the middle of the interface due to the distribution and increases it at the edges of the contact.

The computation time for the semi-analytical contact simulation at the resonance frequency is almost instant since it lasts approximately 2 minutes for a mesh with 51×201 nodes respectively in the X' and Y' directions of the contact interface. In comparison, the contact simulation in the HBM solver takes

approximately 1 minute at each frequency step, with a 5×16 nodes mesh.

5. Influence of wear on the dynamic behaviour

5.1. Wear computation

Using the sliding results obtained with the semi-analytical method at each time-step of the vibration period over the whole interface, it is then possible to estimate wear with accuracy. To do so, a local energy based formulation [17] of the Archard's law [29] is used to compute the wear volume over one vibration cycle:

$$V = \alpha_u \sum_{N_f} \delta_0(N) E_d(N) \tag{18}$$

where V is the wear volume over one period, α_u is the wear coefficient estimated experimentally, N_f is the considered cycle, δ_0 is the tangential displacement and E_d is the dissipated energy. This equation can then be re-expressed to determine the wear depth Δh at every point of the interface after one vibration cycle:

$$\Delta h = \alpha_u \sum_{N_f} \left[\frac{1}{4} \sum_{1cycle} \|\boldsymbol{s}^{(t)}\| \sum_{1cycle} \|\boldsymbol{q}_\tau^{(t)}\| \|\boldsymbol{s}^{(t)}\| \right] \tag{19}$$

where $\boldsymbol{s}^{(t)}$ is the relative displacement between time-steps $(t-1)$ and (t) i.e. the sliding and $\boldsymbol{q}_\tau^{(t)}$ is the shear load at time-step (t). The wear depth Δh is then distributed between both contact surfaces. Moreover, since wear is too small after one cycle, an acceleration factor ΔN is applied by multiplying it with Δh, considering that ΔN cycles are needed before wear modifies the contact behaviour.

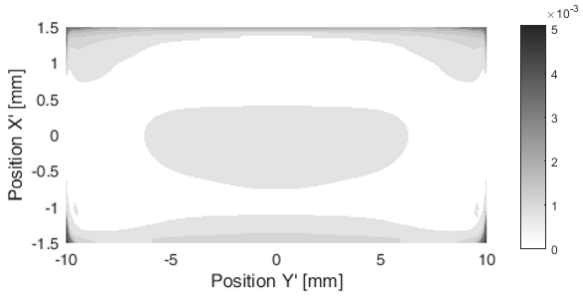

(a) 10^9 vibration cycles

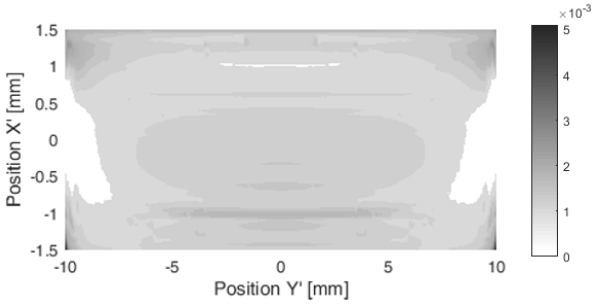

(b) 2.10^9 vibration cycles with geometry update after 10^9 cycles

Figure 9: Wear depth of a contact interface of the blade in [10^{-3} mm]

Figure 9 shows the wear depth after 10^9 vibration cycles (9a) and after 2.10^9 vibration cycles (9b) with a contact geometry update after 10^9 cycle within the semi-analytical contact solver (i.e. $\Delta N = 10^9$). Wear depth after 10^9 cycles is mainly localised within the edges and corners of the interface. After one interface update (Figure 9b) edges and corners wear did not increase. However, wear is more distributed over the whole interface.

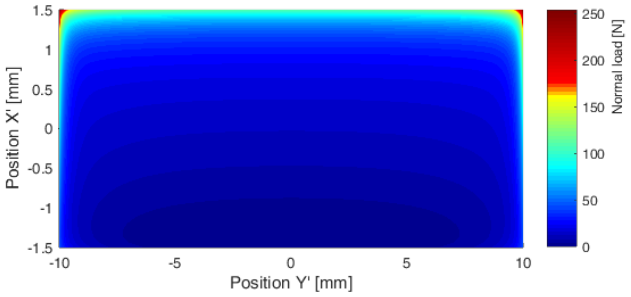

(a) Unworn profile

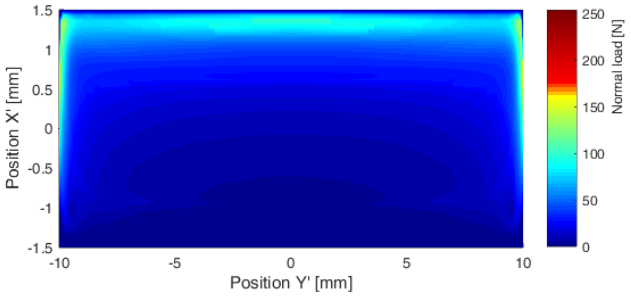

(b) Worn profile after 10^9 vibration cycles

Figure 10: Normal load distribution over the interface for the unworn profile (a) and for the worn profile after 10^9 vibration cycles (b), at one time-step of the dynamic period, computed with the semi-analytical method.

The localisation of wear on the edges and corners means that wear is rounding the edges, decreasing the loads localisation at the same time. Figure 10 represents the normal load distribution over the interface for the unworn profile, and for the worn profile after 10^9 vibration cycles. It can be seen on Figure 10a that the effort is very high on the top corners of the interface, where the effort reaches 257N. However, the loads on the worn profile on Figure 10b are much lower and more distributed over the contact surface. The maximum load has decreased to 166 N and is not localised on the edges anymore.

5.2. Worn geometry dynamic behaviour

The worn profiles previously computed can then be used to update the geometry in the HBM to study the influence of wear on the dynamic response of the bladed-disk. Wear depth is then implemented as a gap $\boldsymbol{G}$ and added in the normal contact law of the DLFT. Hence, the normal part of Equation 10 is reformulated:

$$\tilde{\boldsymbol{\lambda}}^N = \tilde{\boldsymbol{F}}_{\boldsymbol{r}}{}^N - \mathbf{Z}_{\mathbf{r}}{}^N \tilde{\boldsymbol{X}}_{\boldsymbol{r}}{}^N + \epsilon \left(\tilde{\boldsymbol{X}}_{\boldsymbol{r}}{}^N - \boldsymbol{G} - \tilde{\boldsymbol{Y}}_{\boldsymbol{r}}{}^N \right) , \tag{20}$$

where the superscript N stands for "normal" component of the equation.

Figure 11 shows the forced response for the unworn linear (bonded) system, the unworn non linear system and the worn

non-linear responses for the worn profile determined in the previous section, for 10^9 cycles and for 2.10^9 cycles with a geometry update after 10^9 cycles. Non-linear forced responses for the worn profiles are lower than the unworn non-linear forced response. This behaviour can be explained since wear adapts the interfaces hence facilitating sliding and friction dissipated energy. Moreover, the amplitude is slightly smaller after 2.10^9 cycles compared to 10^9 cycle. Considering even more vibrations cycles would then induce more damping on the forced response at the blade's tip.

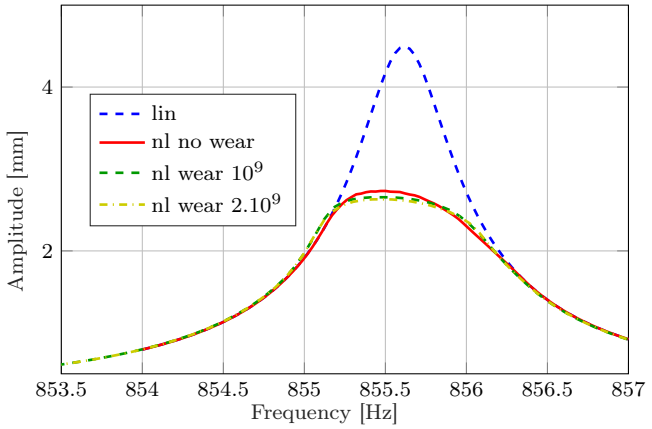

Figure 11: Forced response of the bladed disk for: unworn linear (bonded) (- -), unworn non-linear (——), non-linear worn profile after 10^9 cycles (- -) and non linear worn profile after 2.10^9 (-·-).

6. Conclusion

The work presented in this paper provides a methodology to study the dynamic behaviour of solids in contact, in this case bladed-disks, considering the effect of friction and wear on the dynamic response. The Harmonic Balance Method presented here allows to obtain an accurate dynamic response for the system. However, the mesh cannot be fine enough to study the contact behaviour precisely, which can then be done by using a semi-analytical contact resolution method. Therefore, it was possible to study the interfaces behaviour in detail with a refined mesh and to compute wear with accuracy, while keeping fast computations. Contact phenomena have an important impact on the dynamic response of the bladed disk. Hence, this study allows to compute precisely the vibration levels, helping aircraft engines manufacturers to improve their design.

Several complementary studies are now envisioned to improve and validate this work. First of all, the geometry update frequency in the wear process must be studied, by computing more vibration cycles to determine wear depth. Moreover, these methods must be applied to industrial bladed-disks models to be validated with respect to experiments.

7. Acknowledgement

The authors acknowledge Safran Aircraft Engines for providing the financial support of this project and for giving permission to publish this work. The authors also acknowledge the ANRT for providing the CIFRE grant allowing us to achieve this work.

References

[1] S. Nacivet, C. Pierre, F. Thouverez, L. Jezequel, A dynamic Lagrangian frequency–time method for the vibration of dry-friction-damped systems, Journal of Sound and Vibration 265 (1) (2003) 201–219. doi:10.1016/S0022-460X(02)01447-5.

[2] E. P. Petrov, D. J. Ewins, Effects of Damping and Varying Contact Area at Blade-Disk Joints in Forced Response Analysis of Bladed Disk Assemblies, Journal of Turbomachinery 128 (2) (2005) 403–410. doi:10.1115/1.2181998.

[3] L. Salles, L. Blanc, F. Thouverez, A. Gouskov, Dynamic Analysis of Fretting-Wear in Friction Contact Interfaces, International Journal of Solids and Structures 48 (2010) 1513–1524. doi:10.1016/j.ijsolstr.2011.01.035.

[4] D. Charleux, C. Gibert, F. Thouverez, J. Dupeux, Numerical and experimental study of friction damping blade attachments of rotating bladed disks, International Journal of Rotating Machinery (2006). doi:10.1155/IJRM/2006/71302.

[5] C. W. Schwingshackl, E. P. Petrov, D. J. Ewins, Measured and estimated friction interface parameters in a nonlinear dynamic analysis, Mechanical Systems and Signal Processing 28 (2012) 574–584. doi:10.1016/j.ymssp.2011.10.005.

[6] C. W. Schwingshackl, C. Joannin, L. Pesaresi, J. S. Green, N. Hoffmann, Test Method Development for Nonlinear Damping Extraction of Dovetail Joints, in: Dynamics of Coupled Structures, Volume 1, Conference Proceedings of the Society for Experimental Mechanics Series, 2014, pp. 229–237.

[7] L. Salles, L. Blanc, A. Gouskov, P. Jean, F. Thouverez, Dual Time Stepping Algorithms With the High Order Harmonic Balance Method for Contact Interfaces With Fretting-Wear, Journal of Engineering for Gas Turbines and Power 134 (2014). doi:10.1115/1.4004236.

[8] T. Heinze, L. Scheidt, J. Wallaschek, A. Hartung, Rotational speed-dependent contact formulation for nonlinear blade dynamics prediction, Journal of Engineering for Gas Turbines and Power 141 (4) (2018).

[9] D. Thomas, Dynamics of rotationally periodic structures, International Journal for Numerical Methods in Engineering (1979) 81 – 102.

[10] R. Craig, M. Bampton, Coupling of substructures for dynamic analyses, AIAA journal 6 (7) (1968) 1313–1319.

[11] T. M. Cameron, J. H. Griffin, An Alternating Frequency/Time Domain Method for Calculating the Steady-State Response of Nonlinear Dynamic Systems, Journal of Applied Mechanics 56 (1) (1989) 149–154. doi:10.1115/1.3176036.

[12] E. P. Petrov, D. J. Ewins, Analytical Formulation of Friction Interface Elements for Analysis of Nonlinear Multi-Harmonic Vibrations of Bladed Disks, Journal of Turbomachinery 125 (2) (2003) 364. doi:10.1115/1.1539868.

[13] L. Gallego, B. Fulleringer, S. Deyber, D. Nélias, Multiscale computation of fretting wear at the blade/disk interface, Tribology International 43 (4) (2010) 708–718. doi:10.1016/j.triboint.2009.10.011.

[14] J. Armand, L. Pesaresi, L. Salles, C. W. Schwingshackl, A Multiscale Approach for Nonlinear Dynamic Response Predictions With Fretting Wear, Journal of Engineering for Gas Turbines and Power 139 (2) (2017).

[15] J. Armand, L. Pesaresi, L. Salles, C. Wong, C. W. Schwingshackl, A modelling approach for the nonlinear dynamics of assembled structures undergoing fretting wear, Proceedings of the Royal Society A 475 (2223) (2019) 20180731.

[16] L. Gallego, D. Nélias, C. Jacq, A Comprehensive Method to Predict Wear and to Define the Optimum Geometry of Fretting Surfaces, Journal of Tribology 128 (3) (2006) 476. doi:10.1115/1.2194917.

[17] S. Fouvry, P. Duó, P. Perruchaut, A quantitative approach of Ti–6al–4v fretting damage: friction, wear and crack nucleation, Wear 257 (9) (2004) 916–929. doi:10.1016/j.wear.2004.05.011.

[18] M. Geradin, D. J. Rixen, Mechanical Vibrations: Theory and Application to Structural Dynamics, John Wiley & Sons, 2014.

[19] D. D. Klerk, D. J. Rixen, S. N. Voormeeren, General Framework for Dynamic Substructuring: History, Review and Classification of Techniques, AIAA Journal 46 (5) (2008) 1169–1181. doi:10.2514/1.33274.

[20] R. Craig, C.-J. Chang, Free-interface methods of substructure coupling for dynamic analysis, AIAA Journal 14 (11) (1976) 1633–1635. doi:10.2514/3.7264.
[21] M. Krack, L. Salles, F. Thouverez, Vibration prediction of bladed disks coupled by friction joints, Archives of Computational Methods in Engineering 24 (3) (2017) 589–636. doi:10.1007/s11831-016-9183-2.
[22] G. Kerschen, J.-c. Golinval, A. F. Vakakis, L. A. Bergman, The Method of Proper Orthogonal Decomposition for Dynamical Characterization and Order Reduction of Mechanical Systems: An Overview, Nonlinear Dynamics 41 (1) (2005) 147–169. doi:10.1007/s11071-005-2803-2.
[23] M. Krack, J. Gross, Harmonic Balance for Nonlinear Vibration Problems.
[24] A. E. H. Love, A Treatise on the Mathematical Theory of Elasticity., Vol. 1, 1952.
[25] K. L. Johnson, Contact Mechanics, Cambridge University Press, 1987.
[26] S. Liu, Q. Wang, G. Liu, A versatile method of discrete convolution and FFT (DC-FFT) for contact analyses, Wear 243 (1–2) (2000) 101–111. doi:10.1016/S0043-1648(00)00427-0.
[27] J. J. Kalker, Y. V. Randen, A minimum principle for frictionless elastic contact with application to non-Hertzian half-space contact problems, Journal of Engineering Mathematics 6 (2) (1972) 193–206. doi:10.1007/BF01535102.
[28] I. A. Polonsky, L. M. Keer, A numerical method for solving rough contact problems based on the multi-level multi-summation and conjugate gradient techniques, Wear 231 (2) (1999). doi:10.1016/S0043-1648(99)00113-1.
[29] J. F. Archard, Contact and Rubbing of Flat Surfaces, Journal of applied physics (1953). doi:10.1063/1.1721448.